Supporting Information

Sapir et al. 10.1073/pnas.1414748111

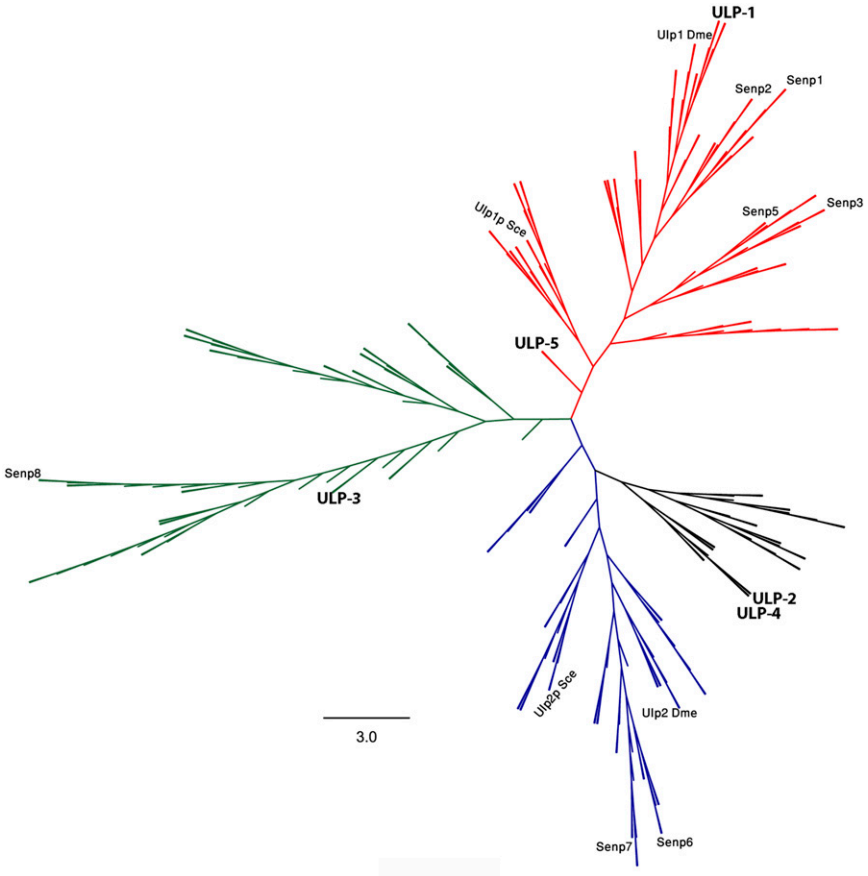

Fig. S1. Phylogenetic tree of *Caenorhabditis elegans* ULPs and other ULPs/SENPs. *C. elegans* ULPs are labeled in bold font. Colors represent different ULP/SENP families. Human SENPs 1–3; 5–8 are shown as well as ULPs of *Drosophila melanogaster* (Dme) and *Saccharomyces cerevisiae* (Sce). (Scale bar: branch length, which is expressed as the expected number of substitutions per site.)

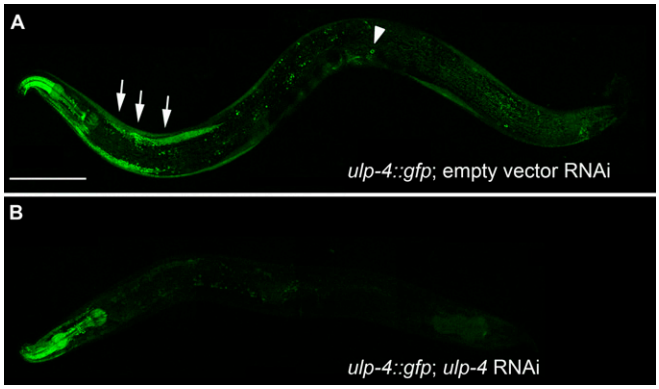

Fig. S2. *ulp-4*::gfp signal is reduced by *ulp-4* RNAi. We tested the activity of *ulp-4* RNAi on worms expressing *ulp-4p*::*ulp-4*::GFP. (*A*) The stereotypic expression pattern of *ulp-4*::GFP in day-1 adult hermaphrodites fed with empty vector RNAi. Hermaphroditic-specific neuron (HSN) expression (white arrowhead) and expression in head muscles (white arrows) are shown. (*B*) *ulp-4* RNAi activity resulted in the elimination of GFP signal from body wall muscle cells and HSN neurons. When the worms were treated with *ulp-4* RNAi for more than two generations, the signal was also reduced in pharyngeal cells. (Scale bar: 50 μm.)

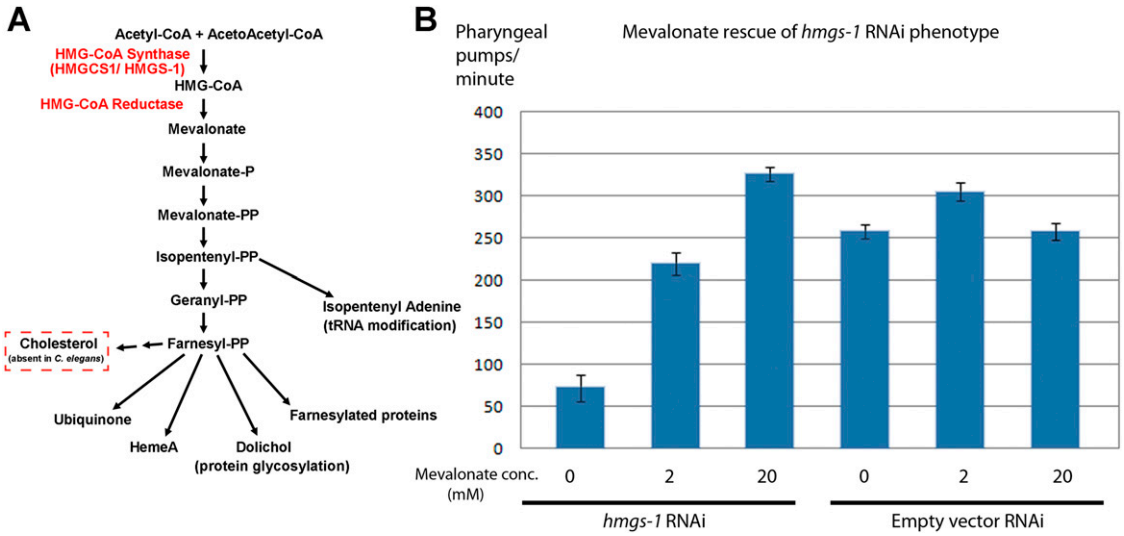

Fig. S3. *hmgs-1* knockdown is rescued by mevalonate supplementation. (*A*) A schematic representation of mevalonate pathway metabolism. Cholesterol production is absent in *C. elegans* but other branches of the pathway are conserved. (*B*) Worms fed with *hmgs-1* RNAi show a significant reduction in the level of pharyngeal pumping. This effect can be fully rescued by supplementation of 20 mM mevalonate indicating that *hmgs-1* knockdown phenotypes stem from impaired mevalonate pathway flux. 20mM mevalonate does not affect the pumping rate of WT worms; precluding a nonspecific rescue by mevalonate supplementation. Bars represent SEs. Number of worms, $n = 10$ WT worms in each condition.

A

Prediction method		SUMOplot			SUMOsp2			SUMO-RF	
C.elegans	Site	Sequence	Score	Site	Sequence	Score	Site	Sequence	Score
HMGS-1	291	GNGVDHKLDENDRA	0.52	408	FTETLQKREVFLRS	3.015	408	FTETLQKREVFLRS	77.11
	314	AQVWKEKTDPYLVF	0.5				314	AQVWKEKTDPYLVF	49.21
	408	FTETLQKREVFLRS	0.5						
	420	RSKEIPKSPSETSL	0.5						
Human									
HMGCS1	305	EAFGDVKLEDTYFD	0.93	105	KSVKTNL	2.853	305	EAFGDVKLEDTYFD	100
	55	IGLGQAKMGFCTDR	0.62	321	AFMKASS	2.265	206	DFYKPDM	61.84
	38	DQAELEKYDGVDAG	0.5	499	PAKKVPR	2.279			
	499	IPSPAKKVPRLPAT	0.37	305	GDVKLED	1.749			
	246	IHAQWQKEGNDKDF	0.33						
	315	FDRDVEKAFMKASS	0.15						
	251	QKEGNDKDFTLNDF	0.15						

B

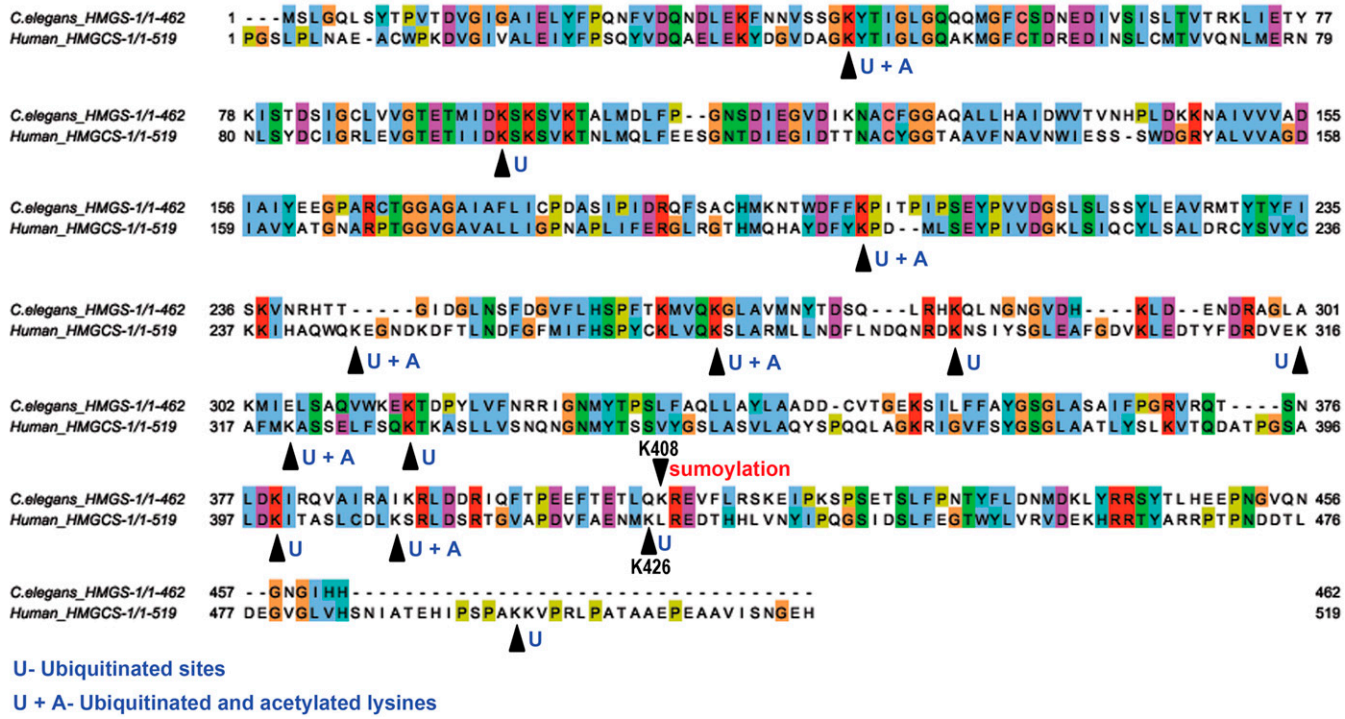

Fig. S4. A comparison between HMGS-1 and human HMG-CoA synthase 1 (HMGCS1) modifications. (*A*) Prediction of sumoylation sites in HMGS-1 and HMGCS1 proteins. Lysine (K) highlighted in red are the residues predicted to be sumoylated. (*B*) HMGCS1 undergoes ubiquitination and acetylation at multiple sites. Human HMGCS1 modifications are based on data available from PhosphoSitePlus (www.phosphosite.org/homeAction.do). Sequences were aligned using ClustalW (www.ebi.ac.uk/Tools/msa/clustalw2) and visualized using Jalview software (1).

1. Waterhouse AM, Procter JB, Martin DM, Clamp M, Barton GJ (2009) Jalview Version 2—a multiple sequence alignment editor and analysis workbench. *Bioinformatics* 25(9):1189–1191.

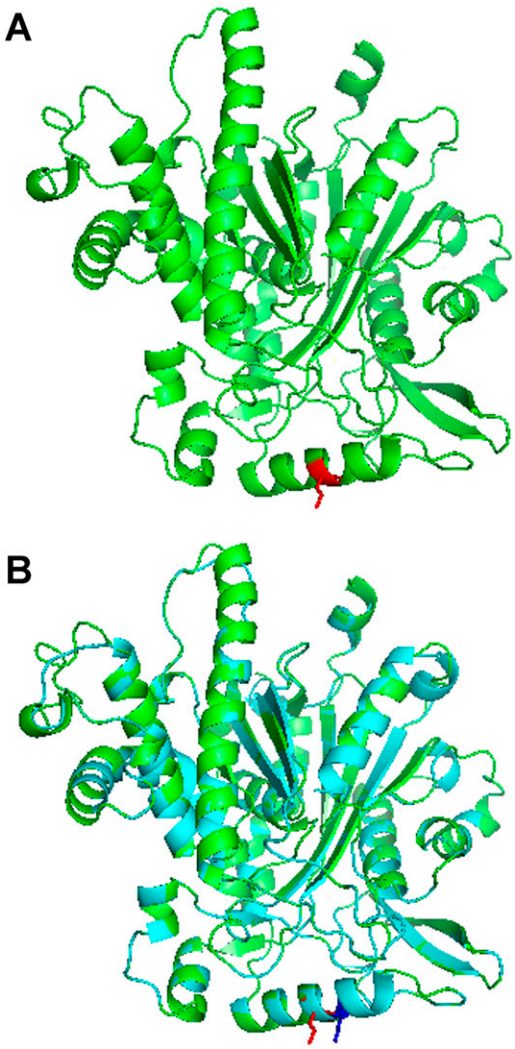

Fig. S5. A model of HMGS-1 structure and its alignment with human HMGCS1. (*A*) Predicted HMGS-1 3D structure based on a Protein Data Bank structural search (www.rcsb.org/pdb/home/home.do). HMGS-1 shares the same structure with the human proteins HMGCS2 (42%) and HMGCS1 (40%) with confidence of 100%. The sumoylated Lys408 is labeled in red. (*B*) Alignment between HMGS-1 and its functional human ortholog HMGCS1. On the HMGCS1 structure, K426 which is the closest to the sumoylated residue of HMGS-1 is labeled in blue. This residue was found to undergo ubiquitination in human HMGCS1. The Phyre server (1) was used to search for proteins with a HMGS-1–related structure.

1. Kelley LA, Sternberg MJ (2009) Protein structure prediction on the Web: A case study using the Phyre server. *Nat Protoc* 4(3):363–371.

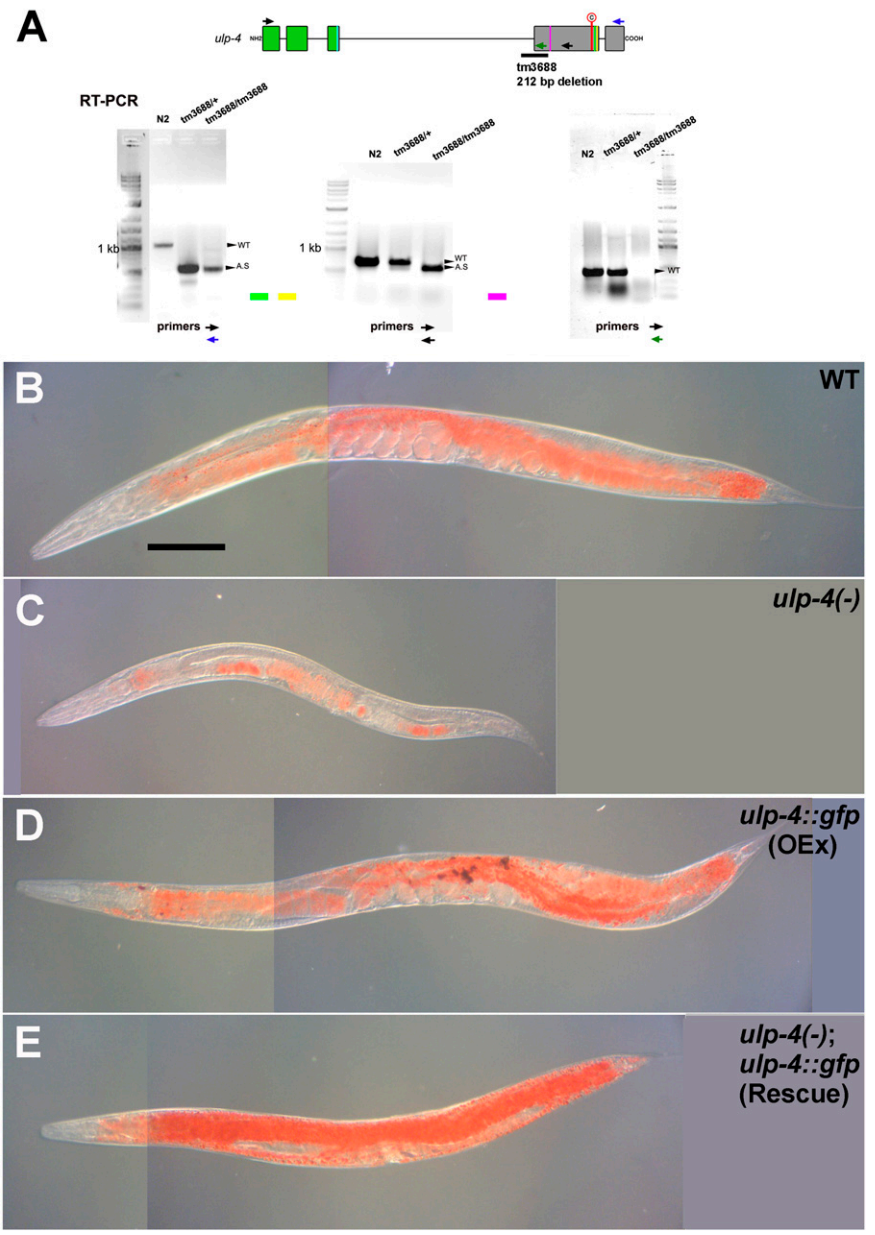

Fig. S6. Molecular characterization of the *ulp-4* locus and its requirement for normal fat homeostasis. (*A*) RT-PCR analyses of *tm3886* within the *ulp-4* locus. The *ulp-4* N-terminal region is in green (exons 1–3). This is followed by the C-terminal region (exons 4–5) that is labeled in gray. This region harbors the *ulp-4* catalytic domain (the conserved cysteine is labeled "©"). RT-PCR analyses revealed that in the strain homozygous for the tm3886 deletion, a truncated transcript still exists. Because the tm3886 deletion introduces a frame shift followed by a stop codon before the catalytic site, this transcript presumably does not code for a functional ULP-4 protein. (*B–E*) Worms' fat level was determined by Oil-O-Red staining. (*C*) *ulp-4*(tm3688) mutant worms have less fat than the WT control (*B*). (*D*) The level of fat is marginally increased in worms overexpressing *ulp-4::gfp*. (*E*) *ulp-4::gfp* construct partially rescues the fat loss of *ulp-4(-)* mutants, indicating that the *ulp-4::gfp* construct is functional. (Scale bar: 50 μm.)

A

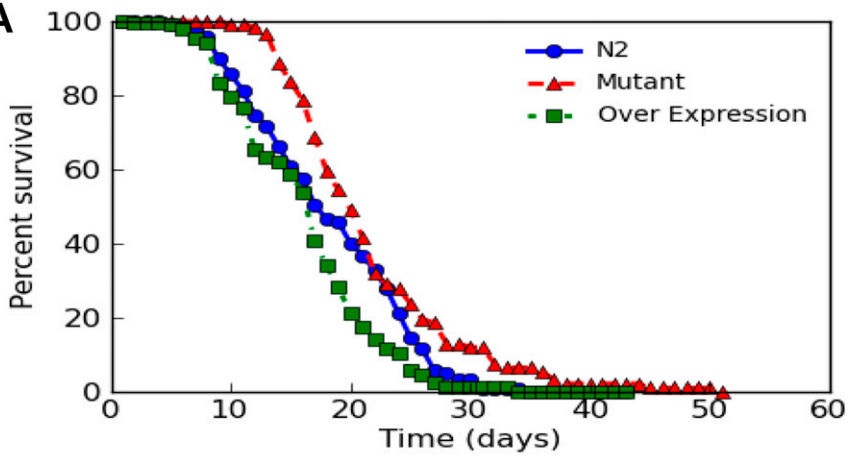

B

Mean/Median Lifespan

		----------Restricted Mean----------			----------Age in days at % mortality----------					
Name	No. of subjects	Days	Std. error	95% C.I.	25%	50%	75%	90%	100%	95% Median C.I.
N2	243	18.28	0.56	17.19~19.37	12	18	24	27	35	16~19
Mutant	152	21.78	0.69	20.44~23.13	17	20	25	32	51	19~21
Over Expression	202	16.26	0.57	15.13~17.38	12	17	20	25	34	15~17

C

Condition	Statistics		
	Chi^2	P-value	Bonferroni P-value
N2 *v.s.* **Mutant**	11.90	0.0006	0.0011
N2 *v.s.* **Over Expression**	7.08	0.0078	0.0156
Mutant *v.s.* **N2**	11.90	0.0006	0.0011
Mutant *v.s.* **Over Expression**	32.35	1.3e-08	2.6e-08
Over Expression *v.s.* **N2**	7.08	0.0078	0.0156
Over Expression *v.s.* **Mutant**	32.35	1.3e-08	2.6e-08

Fig. S7. Opposite effects of *ulp-4* loss and *ulp-4* overexpression (ulp-4::GFP) on *C. elegans* lifespan. (*A*) Lifespan analyses of WT, *ulp-4* mutants, and worms overexpressing *ulp-4* under its own promoter. (*B*) *ulp-4* mutants have a longer median and maximal lifespan than WT controls, whereas *ulp-4* overexpression exhibits an opposite effect. The effect of *ulp-4* on *C. elegans* lifespan is significant based on multiple statistical analyses. (*C*) All lifespan experiments were held at 20 °C on plates seeded with *Escherischia coli*, strain OP50, at the same time.

A

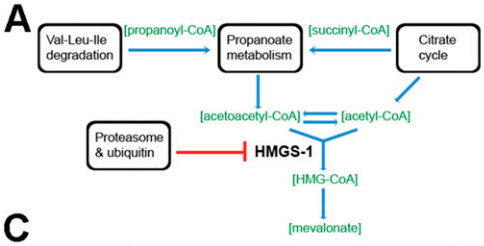

B

KEGG Pathway	Fold enrichment	P-value (Benjamini-corrected)	Number of genes
Ribosome	5.5	1.60E-48	73
Citrate cycle	3.1	0.001	16
VLI degradation	2.8	7.00E-04	19
Propanoate metabolism	2.8	0.014	13
Proteasome	2.4	2.00E-02	15

C

Accession	Description	Coverage (%)	# Unique Peptides	# PSMs	Fold Enrichment
P54871	Hydroxymethylglutaryl-CoA synthase, [HMCS_CAEEL]	55.41	14	107	>>16.8
Q19584	Ubiquitin fusion degradation protein 1 homolog, [UFD1_CAEEL]	48.83	9	46	>>16.8
Q95Y72	Probable 26S proteasome complex subunit dss-1, [DSS1_CAEEL]	23.17	1	1	>>16.8
Q95008	Proteasome subunit alpha type-5, [PSA5_CAEEL]	21.37	3	10	>>16.8
P91430	Ubiquitin-like modifier-activating enzyme 5, [UBA5_CAEEL]	15.27	5	7	>>16.8
Q04908	26S proteasome non-ATPase regulatory subunit 3, [PSMD3_CAEEL]	8.13	3	11	>>16.8
Q20938	Probable 26S proteasome regulatory subunit rpn-6.1, [PS11A_CAEEL]	7.08	2	7	>>16.8
Q966I8	Proteasome subunit beta type [Q966I8_CAEEL]	6.28	1	1	>>16.8
G5ED41	Cullin-associated NEDD8-dissociated protein 1, [CAND1_CAEEL]	3.85	3	4	>>16.8
Q09444	Probable ubiquitin carboxyl-terminal hydrolase, [UBH4_CAEEL]	2.49	1	2	>>16.8
O16368	Probable 26S protease regulatory subunit 4, [PRS4_CAEEL]	16.93	5	15	16.8
Q18787	26S protease regulatory subunit 7, [PRS7_CAEEL]	30.11	10	32	10.8
Q95XX0	Protein UBC-13 (Ubiquitin E2) [Q95XX0_CAEEL]	18.54	1	1	5.6
P46502	Probable 26S protease regulatory subunit 6B, [PRS6B_CAEEL]	24.15	7	30	5.1
P37165	Ubiquitin-like protein 1-40S ribosomal protein S27a, [RS27A_CAEEL]	23.31	2	49	5.0
P0CG71	Polyubiquitin-A, [UBIQ1_CAEEL]	44.63	3	44	4.2
O17071	Probable 26S protease regulatory subunit 10B, [PRS10_CAEEL]	28.82	9	48	3.8
P54811	Transitional endoplasmic reticulum ATPase homolog 1, Cdc48-1, [TERA1_CAEEL]	16.56	4	39	3.6
P54812	Transitional endoplasmic reticulum ATPase homolog 2, Cdc48-2, [TERA2_CAEEL]	10.25	1	28	3.1
O76577	26S proteasome non-ATPase regulatory subunit 14, [PSDE_CAEEL]	11.86	3	19	3.0
Q18231	Protein RPS-30, [Q18231_CAEEL]	8.46	2	13	2.9

Fig. S8. Proteomic analysis of HMGS-1 interactors. (*A*) A diagram of the metabolic network discovered by the survey of HMGS-1 interactors. This analysis suggests that acetyl-CoA and acetoacetyl-CoA synthesis is physically coupled to condensation by HMGS-1, presumably in a hand-off type of mechanism. (*B*) Statistics of the Kyoto Encyclopedia of Genes and Genomes (KEGG, www.genome.jp/kegg) components enriched in the immunoprecipitated fraction based on a KEGG analysis performed with the Database for Annotation, Visualization and Integrated Discovery (DAVID, http://david.abcc.ncifcrf.gov/home.jsp) (1). (*C*) The list of ubiquitin–proteasome-related proteins interacting with HMGS-1. HMGS-1 itself, labeled in red, was found as the most enriched protein in the immunoprecipitated fraction, demonstrating the potency of our assay. The list is comprised of fifteen proteins identified by Eukaryotic Orthologous Groups of proteins analysis (http://genome.jgi-psf.org/help/kogbrowser.jsf) and five proteins that were identified manually.

1. Huang DW, Sherman BT, Lempicki RA (2009) Bioinformatics enrichment tools: Paths toward the comprehensive functional analysis of large gene lists. *Nucleic Acids Res* 37(1):1–13.

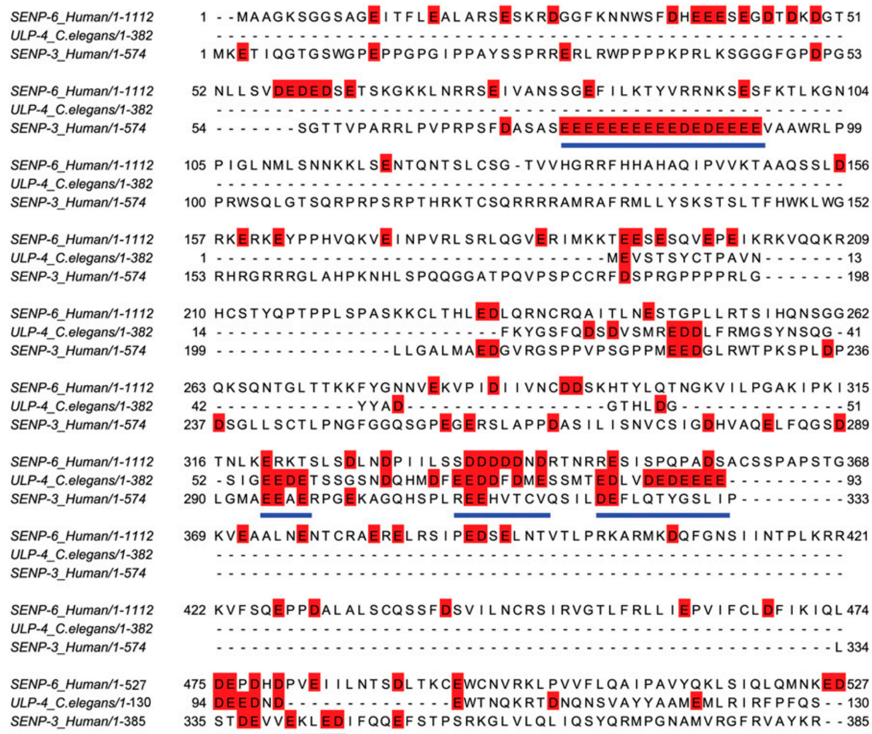

Fig. S9. ClustalW sequence alignment between *C. elegans* ULP-4 small ubiquitin-like modifier protease and human SENP3 and SENP6. Specific acidic residues are labeled in red, and acidic regions (rich in acidic residues) are underlined in blue. Acidic regions are not present in other human SENPs. The alignment was annotated using Jalview software (1).

1. Waterhouse AM, Procter JB, Martin DM, Clamp M, Barton GJ (2009) Jalview Version 2—a multiple sequence alignment editor and analysis workbench. *Bioinformatics* 25(9):1189–1191.

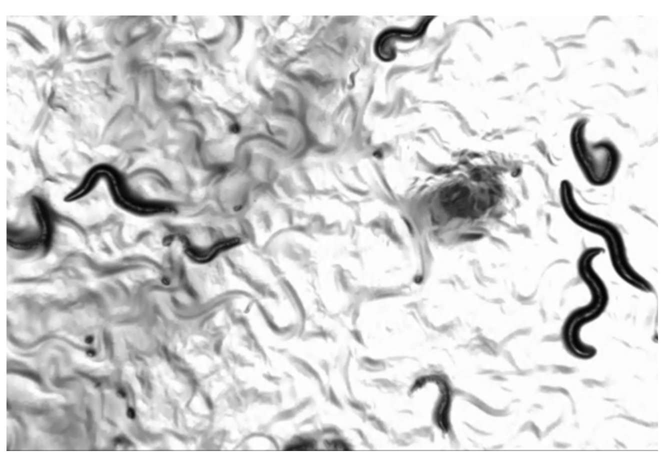

Movie S1. WT worms on *hmgs-1* RNAi. A movie of 30 frames per second showing day-1 adult WT worms grown from egg to adulthood on *hmgs-1* RNAi. Treatment with *hmgs-1* RNAi results in slow development, small body size, partial sterility, and severe worm paralysis.

Movie S1

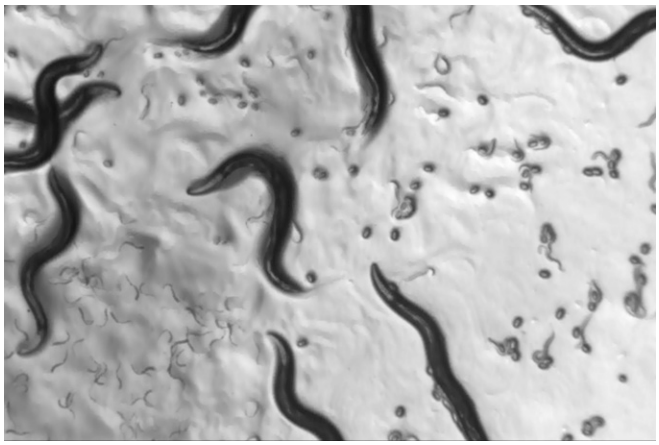

Movie S2. WT worms on *hmgs-1* RNAi with 20 mM mevalonate. A movie of 30 frames per second showing day-1 adult WT worms grown from egg to adulthood on *hmgs-1* RNAi in the presence of 20 mM mevalonate. The severe *hmgs-1* RNAi phenotypes shown in Movie S1 are fully rescued by the supplementation of mevalonate. This rescue demonstrates that *hmgs-1* knockdown phenotypes stem from an impaired mevalonate pathway flux. This result links HMGS-1 activity directly to the mevalonate pathway.

Movie S2

Other Supporting Information Files

Dataset S1 (XLSX)